JOURNAL OF MATERIALS SCIENCE **38** (2003) 1203–1218

Effect of alloying elements on the segregation and dissolution of $CuAl_2$ phase in Al-Si-Cu 319 alloys

Z. LI, A. M. SAMUEL, F. H. SAMUEL
Département des Sciences Appliquées, Université du Québec à Chicoutimi, 555, Boulevard de l'Université, Chicoutimi (Québec), Canada G7H 2B1
E-mail: fhsamuel@uqac.ca

C. RAVINDRAN
Department of Mechanical, Aerospace and Industrial Engineering, Ryerson University, 350 Victoria Street, Toronto, Canada M5B 2K3

S. VALTIERRA
Research and Development, Corporativo Nemak, P.O. 100 Bosques del Valle, Garza Garcia, N.L. 66221, Mexico

The hypoeutectic 319 aluminum alloy (Al-7%Si-3.5%Cu) was used in the present study to investigate the effect of diverse alloying elements on the dissolution of the copper phase ($CuAl_2$) during solution heat treatment. Elements such as Sr, Fe and P were added to the base alloy individually and in various combinations. The cooling curves of these alloys were obtained by solidifying the alloy melts in a preheated graphite mold (600°C, cooling rate ~0.8°C/s). From these the first derivate curves were plotted and used to determine the effect of the additives on the precipitation temperature of the Al-$CuAl_2$ eutectic reaction. Microstructural examination was carried out using optical microscopy, image analysis, and electron probe microanalysis (EPMA), with energy dispersive X-ray (EDX) and wavelength dispersive spectroscopic (WDS) analysis facilities. Samples from different alloys were solution heat treated at 505°C for various times up to 100 hours. The results explicitly reveal that solution heat treatment plays a critical role on the dissolution of the $CuAl_2$ phase. It is found that Sr leads to segregation of the $CuAl_2$ phase away from the Al-Si eutectic regions, which slows down its dissolution during solution heat treatment. The β-Al_5FeSi phase platelets act as preferred precipitation sites for the copper phase and hence lessen the degree of segregation. Thus, addition of Fe can accelerate the copper phase dissolution. However, phosphorus addition has a negative effect on $CuAl_2$ dissolution due to (i) its solubility in the $CuAl_2$ phase particles, and (ii) the formation of $(Al,P)O_2$ oxide particles which act as nucleation sites for the precipitation of the block-like $CuAl_2$ phase. It retards the complete dissolution of this copper phase even after 100 hr solution treatment. In the case when phosphorus and iron are added together, the negative effect of phosphorus can be neutralized to some extent.

1. Introduction

The excellent castability and mechanical properties of 319 aluminum alloy makes it a popular foundry alloy for use in automotives applications. Its low specific gravity is essential to reduce energy consumption, and its excellent corrosion resistance and low costs of recycling are also important considerations from an environmental point of view [1]. Based on the aluminum-silicon (Al-Si) system, the alloy contains copper (Cu) and magnesium (Mg) as the main alloying elements. Addition of Cu to eutectic Al-Si alloys leads to a slight increase in the alloy fluidity, and a depression in the Si eutectic temperature of ~1.8°C for every 1 wt% Cu added. Also, some of the mechanical properties obviously benefit from the addition of Cu as an alloying element (such as YS and UTS) [2].

It is well known that at ~548°C, the amount of Cu in solid solution in Al is about 5.7 wt%. This value decreases with decreasing temperature, reaching 0.1–0.2 wt% at 250°C [3]. Copper forms an intermetallic phase with Al that precipitates during solidification either as block-like $CuAl_2$ or in eutectic form as $(Al + CuAl_2)$. In 319 alloys, the copper intermetallic phase precipitates in these two forms, according

to a multicomponent eutectic reaction reported by Mondolfo [4]:

$$L \rightarrow Al + CuAl_2 + \beta\text{-}Al_5FeSi + Si \quad \text{at } 525^\circ C$$

Iron (Fe) is one of the most critical alloying elements for 319 alloys. During solidification, it forms several intermetallic compounds. Among these, the formation of hard brittle plates of the β-Al_5FeSi phase is particularly deleterious to the alloy mechanical properties [5]. Thus when the Fe level in 319 alloys is higher than 1.5%, the alloy should either be scrapped or diluted with a low-Fe alloy to lower the iron level and reduce the possibility of the precipitation of an excessive amount of β-platelets [6]. There are two ways in which the presence of Fe contributes to the hardening of Al-Si alloys: one is attributed to Fe-related natural aging processes; the other is caused by the dispersion of massive Fe-rich phases throughout the matrix. Iron intermetallics, especially in the form of the β-Al_5FeSi phase, act as nucleants for the $CuAl_2$ phase [7].

Currently, strontium (Sr) is commonly employed in Al-Si casting alloys to modify the eutectic silicon morphology from a coarse, flake-like to a fine fibrous form. The change in the Si morphology, in turn, improves the alloy mechanical properties, particularly ductility [8]. It is now widely accepted that strontium atoms that are incorporated into the crystal structure of silicon enhance the formation of growth twins and allow the silicon to bend and twist into a fibrous morphology [9]. Also, modification with Sr considerably lowers the eutectic reaction temperature. The depression in the eutectic temperature can be used as an indicator of the extent of Si structure modification expected in the casting: the lower the eutectic temperature, the greater the modification effect [10–12]. However, Sr modification also results in a larger area fraction of the interdendritic blocky $CuAl_2$ structure [13].

It has been observed that the presence of Sr also leads to segregation of the copper phase in areas away from the Al-Si eutectic regions, resulting in slowing its dissolution during solution heat treatment. Also, due to the segregation, the $CuAl_2$ phase precipitates in the blocky form rather than in the fine eutectic form [14]. Compared with the latter, the blocky phase is more difficult to dissolve into the aluminum matrix. It can be reasonably presumed that the mechanism of $CuAl_2$ precipitation is caused by a divorced eutectic reaction that is coupled with segregation in the remaining areas shaped by the advancing eutectic Si-containing interdentric regions [9].

When the solution heat treatment temperature applied to 319 alloys exceeds the melting point of the copper phase, there will be localized incipient melting of the phase at the grain boundaries, resulting in the formation of shrinkage cavities when the alloy samples are quenched after solution heat treatment. This process is expected to lead to reduction in the mechanical properties. Studies by Gauthier *et al.* [15, 16] on the solution heat treatment and aging behavior of 319 alloy over a temperature range of 480°C to 540°C, for solution times of up to 24 hours, showed that the best combination of tensile strength and ductility was obtained when the as-cast material was solution-heat-treated at 515°C for 8 to 16 hours, followed by quenching in warm water at 60°C. A higher solution temperature was seen to result in the partial melting of the copper phase, the formation of a structureless form of the phase and related porosity on quenching, with a consequent deterioration of the tensile properties. A two-stage solution heat treatment suggested by Sokolowski *et al.* [17] is reported to significantly reduce the amount of copper-rich phase in the 319 alloys, give rise to better homogenization prior to aging, and improve the mechanical properties.

The present study was undertaken to investigate the precipitation behavior of the $CuAl_2$phase in various 319 type alloys containing Sr, Fe and P, individually or in combination, and its dissolution during solution heat treatment at 505°C for times up to 100 h.

2. Experimental procedure

Measured quantities of pure aluminum, silicon and Al-33% Cu master alloy were used to prepare the experimental Al-7% Si-3.5% Cu base alloy. The melt was poured into ingots. The chemical composition is shown in Table I. The base alloy ingots were cut into small pieces, dried, and melted in a 1-kg capacity SiC crucible heated by means of an electric resistance furnace. The melting temperature was kept at 725°C ± 5°C. Strontium was added in the form of Al-10% Sr master alloy (~200 ppm). Iron was introduced in the form of Al-25% Fe master alloy. The melt was degassed for ~15 minutes to ensure homogeneous mixing of the additions. The different experimental alloys and their respective codes are listed in Table II.

Similar experiments were carried out using industrial 319 alloy. In this case, phosphorus was also added (in addition to Sr and Fe) using Cu-8% P brazing alloy. The corresponding alloy codes are shown in Table II.

In order to determine the possible reactions that could take place during solidification under conditions close to equilibrium (~0.8°C s^{-1}), the liquid metal was poured into a graphite crucible (length: 10 cm, diameter: 6 cm) that was preheated at 600°C. Thermal analysis was carried out simultaneously, using a K-type thermocouple (chromel-alumel) placed vertically within the mold (through a hole in the bottom of the mold) with its tip at ~30 mm above the bottom,

TABLE I Chemical compositions (wt%) of the experimental base alloy (coded ASC) and industrial 319 alloy

	Element concentration (wt%)											
Alloy	Si	Fe	Cu	Mn	Mg	Zn	Al	Cr	Ti	Sr	B	Ni
ASC	6.50	0.1245	3.054	<0.0005	0.0018	<0.0017	90.3	<0.0005	<0.0013	<0.0000	<0.0002	<0.0016
319 alloy	5.95	0.11	3.56	0.02	0.043	<0.01	90.16	0.001	0.145	–	–	0.01

TABLE II List of the alloys used in the present work and their respective codes

Alloy type	Alloy code	Nominal composition
Experimental alloy	ASC	Al-7%Si-3.5%Cu (Base alloy)
	ASCS	Base alloy + Sr
	ASCF	Base alloy + 1%Fe
	ASCFS-1	Base alloy + 0.9%Fe + Sr
	ASCFS-2	Base alloy + 1.2%Fe + Sr
Industrial alloy	H4T1	319 alloy + Sr + 60 ppm P
	H20T1	319 alloy + Fe + Sr + 90 ppm P

*Sr additions: 150–200 ppm.

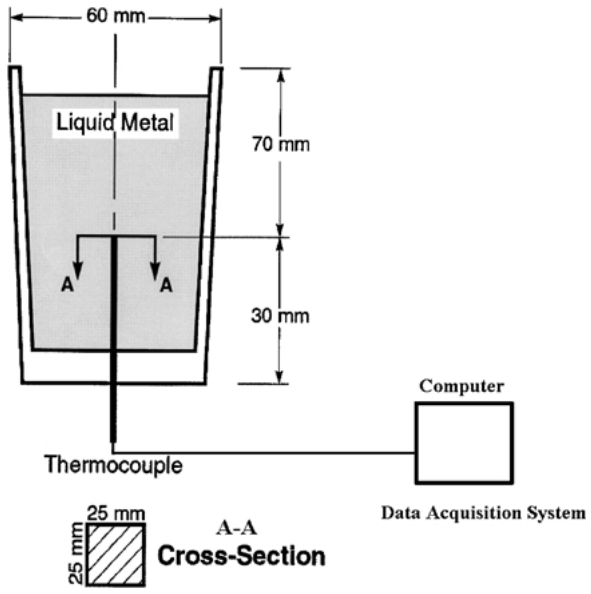

Figure 1 Schematic diagram of the graphite mold used for thermal analysis.

and interfaced with a personal computer (see Fig. 1). The temperature-time data was recorded by means of a data acquisition system attached to the computer (at a rate of 0.2 sec). From the thermal analysis data, the cooling curves and their first derivatives were plotted using Microsoft Excel software. Samplings for chemical analysis were also taken simultaneously for each melt condition. The actual alloying element addition for the various alloys, as obtained from the chemical analysis are listed in Table III.

Eight samples (2.5 cm × 2.5 cm) for metallographic examination were sectioned from each alloy casting (from a bigger section sliced from the central part containing the thermocouple tip). One of these (as-cast condition) was mounted in bakelite, and polished to a fine finish (1μm diamond paste). The other samples were solution heat-treated at 505°C in a forced-air furnace (where the temperature could be controlled to within ±2°C) for different solution times, i.e., 4, 8, 12, 24, 48, 72 and 100 hours. After solutionizing, the samples were immediately quenched in hot water (~60°C) to stop any further reaction of the copper phase. These samples were then mounted and polished. Optical micrographs were taken at magnifications 200× and 750× for each sample.

Microstructural changes were examined and quantified using a Leco 2001 image analyzer in conjunction with the optical microscope (Olympus PMG3), to measure the amount of undissolved $CuAl_2$ phase following the different solution treatment times applied. In each case, fifty fields were measured over the entire sample surface (in a systematic fashion) and the percentage area of $CuAl_2$ phase was measured in each field. From these readings, the average area percent of undissolved $CuAl_2$ phase was determined for each condition. In addition, the dissolution behavior was also studied using an electron probe microanalyzer (EPMA) equipped with EDX and WDS facilities, operating at 20 kV (the size of the analyzed zone was ~2 μm).

TABLE III Actual alloying element additions (wt%) in the alloys studied obtained from chemical analysis

	Main alloying elements			
Alloy code	Cu	Fe	Sr	P
ASC	3.054	0.1245	<0.0000	—
ASCS	2.990	0.1190	0.0060	—
ASCF	2.970	1.015	<0.0000	—
ASCFS-1	3.080	0.862	0.0063	—
ASCFS-2	2.820	1.200	0.0140	—
H4T1	3.56	0.11	0.0140	0.0019
H20T1	3.39	0.68	0.0126	0.0033

3. Results and discussion

3.1. Thermal analysis

From the first derivative curves obtained from the cooling curves of each of the alloys studied, the precipitation temperatures of Al + $CuAl_2$ eutectic were noted and are listed in Table IV. The temperatures of this eutectic reaction in the base alloy (coded as ASC) and ASCF alloy (containing 1 wt% Fe) are lower than that obtained in the Sr-containing or (P + Sr)-containing alloys (viz., ASCS, H4T1, H20T1 alloys). This difference can be due to the fact that the strontium modification leads the Al-$CuAl_2$ eutectic reaction to take place somewhat earlier, i.e., $CuAl_2$ particles are much easier to nucleate during solidification in the case of Sr modification.

The cooling curves and first derivatives obtained from ASC, ASCS and ASCF alloys are shown in Fig. 2, while the corresponding reactions expected to occur are listed in Table V. Apparently, the precipitation of the β-phase prevents the segregation of the $CuAl_2$ phase through its nucleation along the long sides of the β-phase platelets. However, it has no effect on the precipitation temperature of Al + $CuAl_2$ eutectic, which can be noted by comparing the base alloy to ASCF

TABLE IV Precipitation temperatures of Al-$CuAl_2$ eutectic in the alloys studied

Alloy code	Temperature (°C)
ASC	509
ASCS	516
ASCF	509
ASCFS-1	516
ASCFS-2	515
H4T1	517
H20T1	518

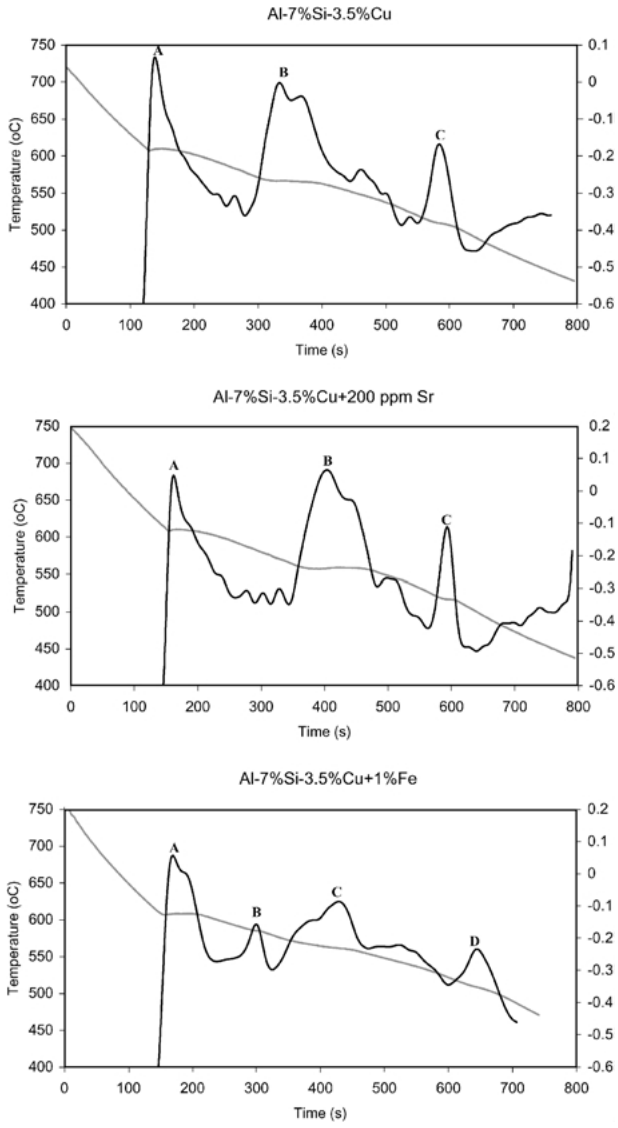

Figure 2 Cooling curves and first derivatives obtained from ASC, ASCS and ASCF alloys.

alloy. In the Sr-modified base alloy (viz., ASCS alloy), however, the solidification temperature increases to 516°C, where the strontium pushes the $(Al + CuAl_2)$ eutectic particles away from the well-modified silicon particles i.e., segregates them into clusters. In this case the $CuAl_2$ particles solidify earlier compared to the base alloy (viz., ASC alloy). At the same time, it is interesting to note that the precipitation temperature of $CuAl_2$ is almost stable even when iron and phosphorus are added to the Sr-modified base alloy (cf. ASCS and ASCFS alloys). Thus it can be reasonably deduced that the modification function of strontium is fundamental in Al-Si-Cu 319 type alloys, as it is observed to dominate the segregation of the copper phase in all the alloys studied.

TABLE V Expected reactions in ASC, ASCS and ASCF alloys

Alloy code	Peak	Temperature (°C)	Reaction
ASC	A	608	Precipitation of α-Al dendrite network
	B	566	Al-Si eutectic reaction
	C	509	Al-$CuAl_2$ eutectic reaction
ASCS	A	609	Precipitation of α-Al dendrite network
	B	558	Al-Si eutectic reaction
	C	516	Al-$CuAl_2$ eutectic reaction
ASCF	A	605	Precipitation of α-Al dendrite network
	B	581	Precipitation of β-Al_5FeSi phase
	C	564	Al-Si eutectic reaction
	D	509	Al-$CuAl_2$ eutectic reaction

3.2. Optical microscopy

Fig. 3a shows the as-cast microstructure of the base ASC alloy, in which the copper phase is seen mainly as small pockets of $(Al + CuAl_2)$ eutectic or the blocky $CuAl_2$ phase, nucleating on preexisting particles, i.e., coarse Si particles or β-Al_5FeSi platelets. Similar observations have been reported by Samuel *et al.* [18]. The arrows marked B and C indicate two instances of such Si particle nucleation sites on which the $(Al + CuAl_2)$ particles are seen to occur. A high magnification micrograph, Fig. 3b, shows the details of the $(Al + CuAl_2)$ eutectic particle marked A in Fig. 3a. When strontium is added to the alloy (viz., ASCS alloy), the eutectic silicon particles become much finer compared to those observed in the base alloy, Fig. 4. The addition of Sr also leads to clustering of the $CuAl_2$ particles in regions away from the growing Al-Si eutectic colonies. Fig. 4 reveals that the $CuAl_2$ phase solidifies in the blocky form rather than in the eutectic one due to Sr-modification.

The microstructure of the ASCF alloy is exhibited in Fig. 5, where a large number of β-Al_5FeSi platelets can be seen in the matrix, decorated by the $(Al + CuAl_2)$ particles. The microstructures of ASCFS-1 (Fig. 6) and ASCFS-2 (Fig. 7) alloys show that the β-phase and the blocky $CuAl_2$ phase are connected to each other, viz., the β-platelets act as nucleation sites for the copper phase particles. Due to the presence of Sr in the alloy, the two phases occur in regions away from those occupied by the (well-modified) Al-Si eutectic. Also, on account of its higher Fe content, the ASCFS-2 alloy (Fig. 7) displays a larger amount of the β-Al_5FeSi phase compared to ASCFS-1 alloy.

Fig. 8 shows the microstructure of H4T1 alloy (industrial 319 alloy with Sr and P additions), where $CuAl_2$ and AlP particles are observed along the dendrite cell boundaries. When the Fe level of the alloy is increased (viz., H20T1 alloy), the corresponding microstructure, Fig. 9, shows no obvious differences when compared to that of the ASCFS-2 alloy (Fig. 7). Thus, from Figs 7, 8 and 9, it can be concluded that the changes in the microstructure of 319 alloys brought out by the addition of P are not very obvious in the presence of other element additions, such as Fe and Sr. However, the $CuAl_2$ particles still have the tendency to precipitate on the β-Al_5FeSi platelets.

3.3. Dissolution of $CuAl_2$ during solution heat treatment

Solution heat treatment causes fragmentation and spheroidization of the silicon particles which are

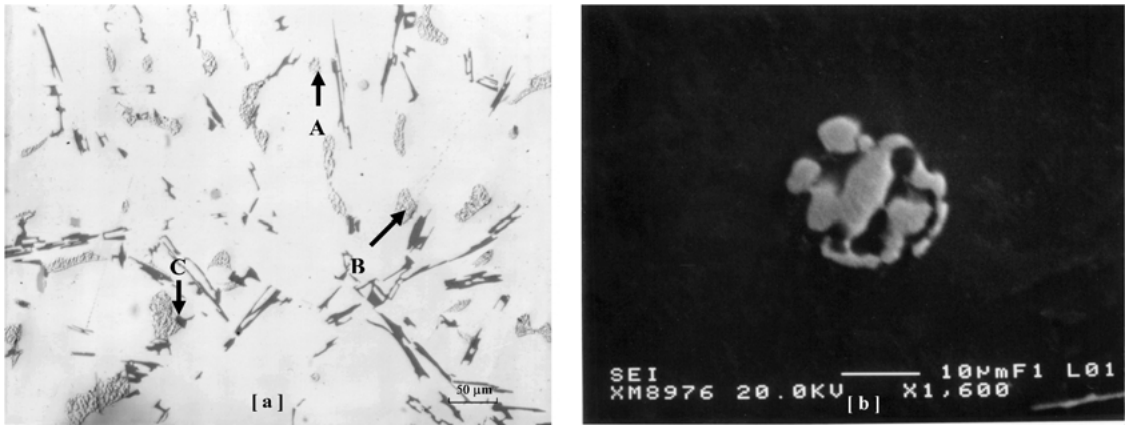

Figure 3 (a) Microstructure of the experimental base alloy (ASC) in the as-cast condition; (b) High magnification micrograph showing the eutectic-like copper phase marked A in (a).

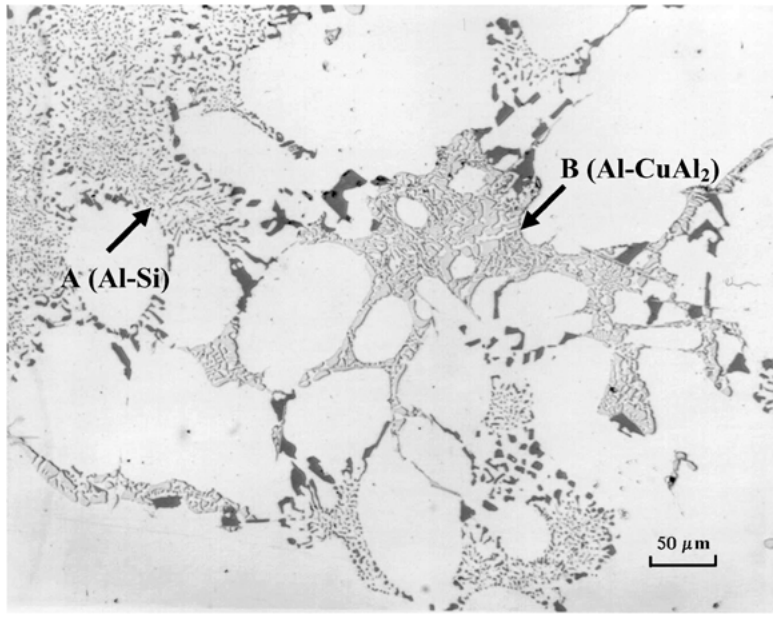

Figure 4 As-cast microstructure of ASCS alloy (Sr modified base alloy), showing Al-Si eutectic (A), and $CuAl_2$ segregation (B).

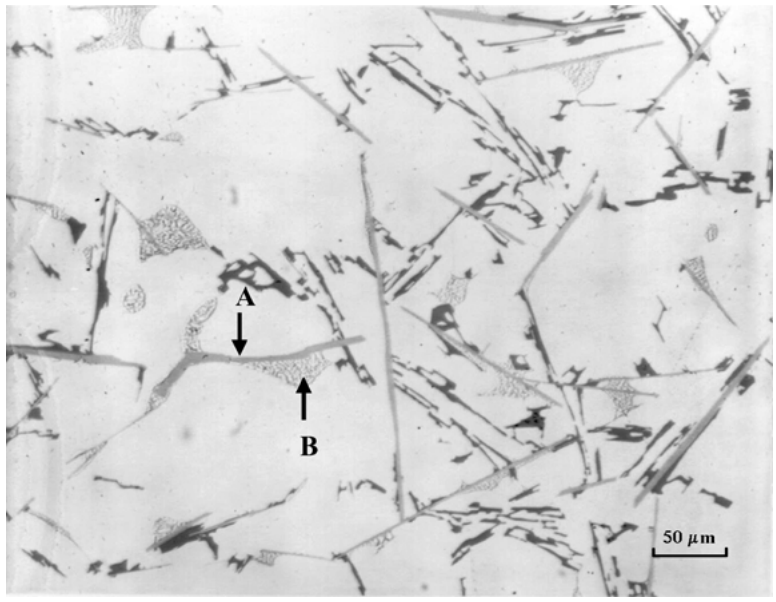

Figure 5 As-cast microstructure of ASCF alloy (base alloy containing 1 wt% Fe), showing a β-Al_5FeSi platelet (A), and eutectic ($Al + CuAl_2$) precipitated along the side of the β-phase (B).

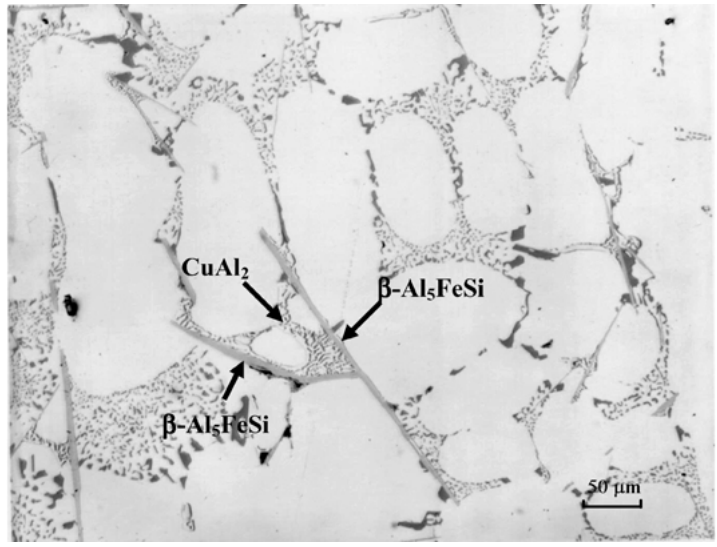

Figure 6 As-cast microstructure of ASCFS-1 alloy (base alloy containing 0.9 wt% Fe and modified with Sr). Note how the β- and Cu-phases occur away from the Al-Si eutectic regions.

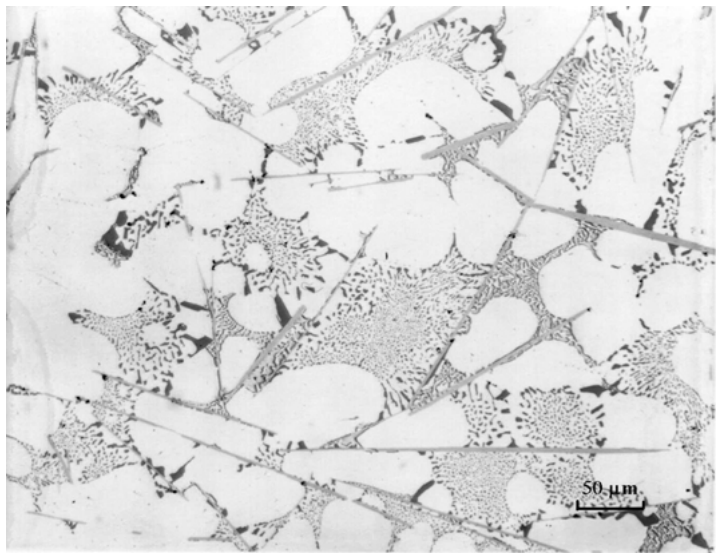

Figure 7 As-cast microstructure of ASCFS-2 alloy (base alloy containing 1.2 wt% Fe and modified with Sr). Note the larger amount of β-platelets compared to Fig. 6.

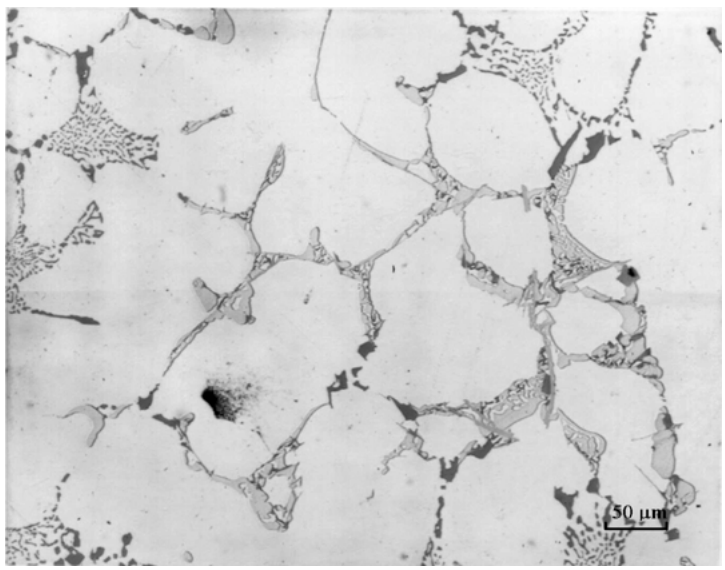

Figure 8 As-cast microstructure of H4T1 alloy (industrial 319 alloy containing 60 ppm P and modified with Sr), showing the precipitation of the $CuAl_2$ phase along the dendrite cell boundaries.

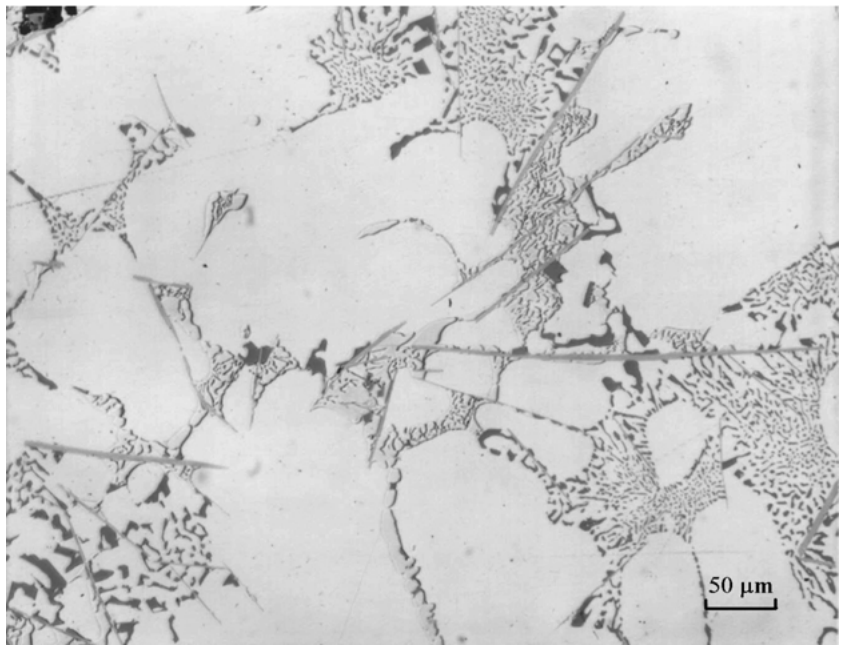

Figure 9 As-cast microstructure of H20T1 alloy (industrial 319 alloy containing 90 ppm P, 0.7 wt% Fe and modified with Sr), showing a structure similar to that of Fig. 7.

beneficial to the resultant alloy mechanical properties. At the same time, strontium modification has also been found to considerably lower solution treatment times [19].

Table VI shows the Al and Cu concentrations obtained in $CuAl_2$ particles observed in the experimental Al-7% Si-3.5% Cu alloy in the as-cast condition ($\sim$0.8°C/s). The six spots listed include all possible $CuAl_2$ morphologies existing in the sample. The data shows that the composition of $CuAl_2$ is nearly stable regardless its form. Again, it is necessary to point out that the morphology of the $CuAl_2$ particles will depend on the segregation or dispersion caused by the presence of the added elements, with no significant effect on the stoichiometric composition of the $CuAl_2$ phase itself.

As mentioned previously, copper forms an intermetallic phase with aluminum that precipitates during solidification either as block-like $CuAl_2$ or in eutectic form as ($Al + CuAl_2$). These phases are easily distinguishable under an optical microscope. In order to study the effect of solution heat treatment, the percentage area of undissolved $CuAl_2$ phase was measured for the various alloy samples/conditions. A Leco 2001 image analyzer was used in conjunction with the optical microscope for quantitative analysis. The amounts of undissolved $CuAl_2$ phase so determined were plotted as a function of solution heat treatment time and are presented in Figs 10 through 16.

TABLE VI Al and Cu concentrations (at.%) of $CuAl_2$ phase in the experimental Al-7%Si-3.5%Cu alloy (as-cast condition; cooling rate $\sim$0.8°C/s)

Spot no.	Al	Cu
1	68.994	29.850
2	68.702	30.194
3	72.106	27.021
4	63.765	27.469
5	69.117	29.799
6	75.002	23.031

Fig. 10 reveals the progress of $CuAl_2$ phase dissolution in the experimental ASC base alloy. After 4 hours' solution treatment at 505°C, the quantity of $CuAl_2$ phase decreases abruptly from 2.6% to 0.77%, i.e., about 70% of the total $CuAl_2$ phase has been dissolved in the matrix. With further solution treatment, up to 48 h, the $CuAl_2$ phase dissolves very slowly, reaching 0.03%. Prolonged solution treatment, i.e., 100 h, tends to put the rest of the copper into the surrounding aluminum matrix. It should be mentioned here that the term "complete dissolution" is taken to mean that the $CuAl_2$ particles cannot be detected in the matrix by optical means (at 500X magnification).

In the case of the modified alloy (viz., ASCS alloy, Fig. 11), most of the $CuAl_2$ ($\sim$2.7%) is dissolved after 12 hours. Thereafter, the percentage of the remaining $CuAl_2$ phase ($\sim$0.5%) reduces slowly with further increase in solution time. Compared to the base alloy (ASC), the amount of undissolved $CuAl_2$ phase in the ASCS alloy was about 20% higher in the as-cast condition. This is to be expected, as the Sr-modification should obviously slow down the rate of $CuAl_2$ dissolution due to its effect on the segregation of the $CuAl_2$ phase during solidification.

Comparing Fig. 12 (ASCF alloy) with Fig. 10 (ASC alloy), the addition of Fe shortens the time needed for dissolution of the $CuAl_2$ phase to 24 hours, i.e., almost half of the time needed in the case of the base alloy to reach the same level of dissolution. The addition of Fe to the base alloy assists in the dispersion of the $CuAl_2$ particles, since the β-Al_5FeSi phase, which precipitates before the Al-$CuAl_2$ eutectic (as inferred from the corresponding cooling curve) provides nucleation sites for the $CuAl_2$ particles. Consequently, there is much less tendency for $CuAl_2$ phase segregation to occur, leading

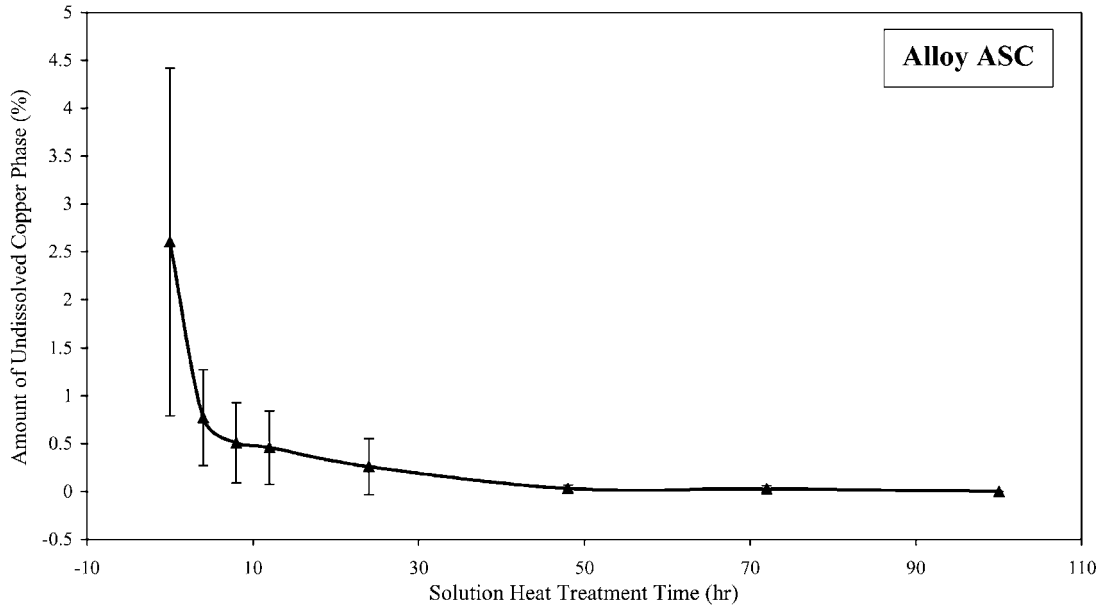

Figure 10 $CuAl_2$ phase dissolution in ASC alloy during solution heat treatment at 505°C as a function of solution treatment time.

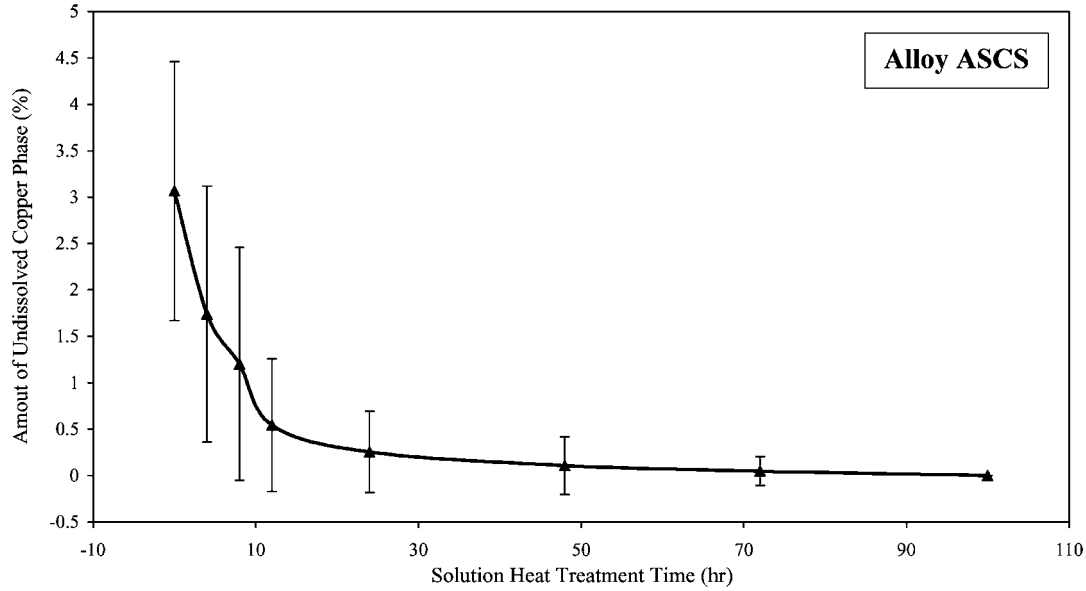

Figure 11 $CuAl_2$ phase dissolution in ASCS alloy during solution heat treatment at 505°C as a function of solution treatment time.

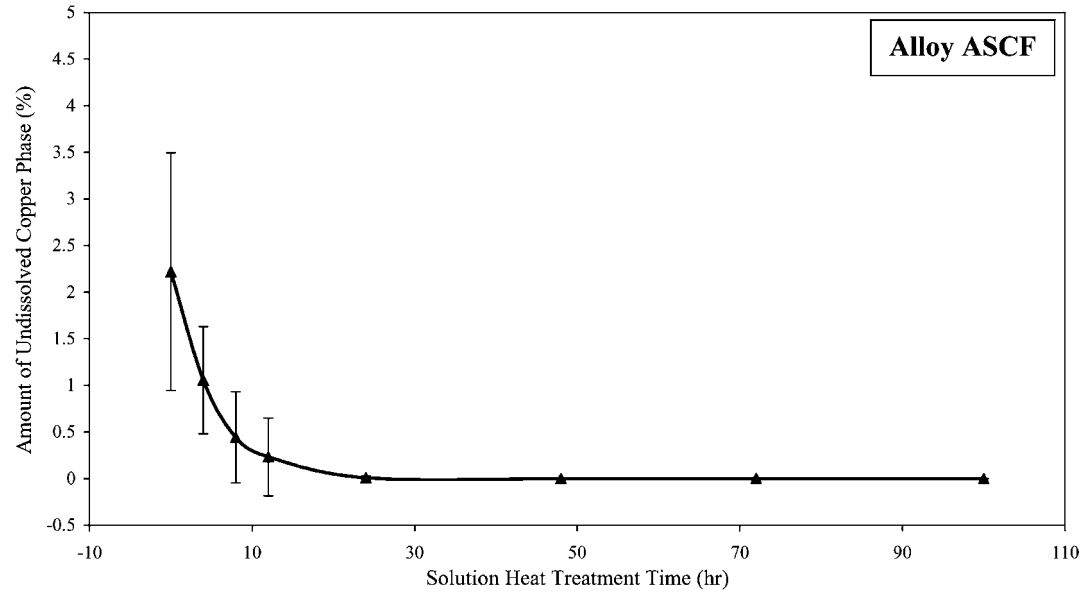

Figure 12 $CuAl_2$ phase dissolution in ASCF alloy during solution heat treatment at 505°C as a function of solution treatment time.

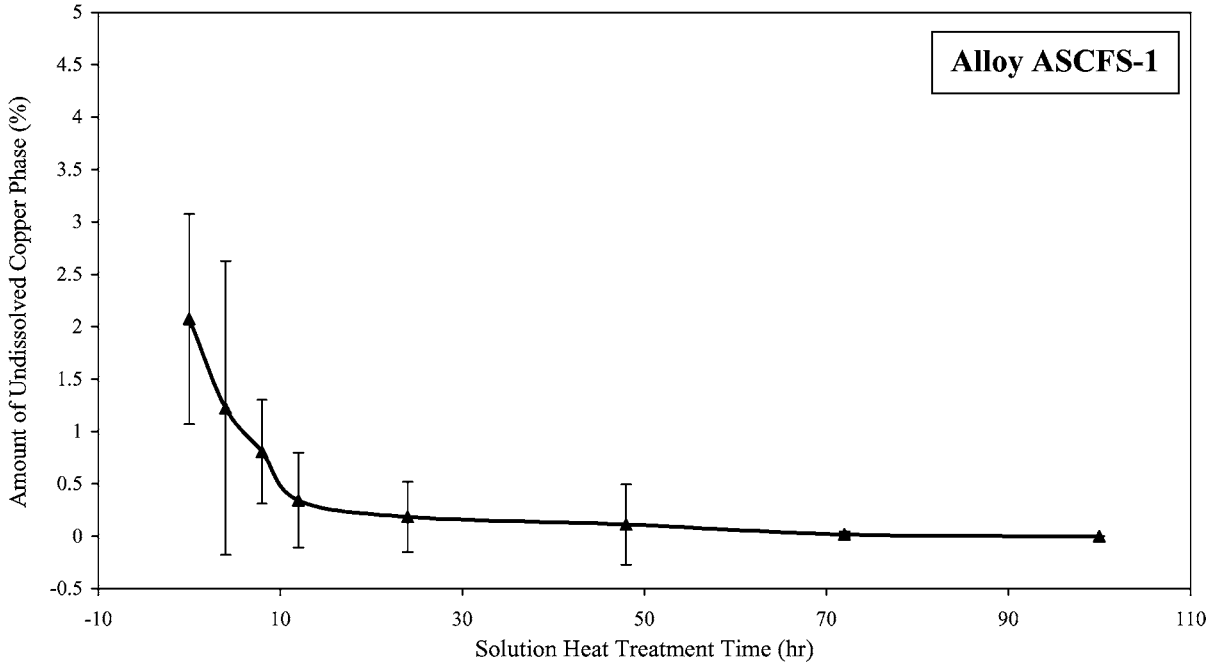

Figure 13 $CuAl_2$ phase dissolution in ASCFS-1 alloy during solution heat treatment at 505°C as a function of solution treatment time.

to smaller $CuAl_2$ particle sizes. Thus, during solution heat treatment, these $CuAl_2$ particles will be much more easily dissolved.

The ASCFS-1 alloy and the ASCFS-2 alloy (Figs 13 and 14, respectively) have more or less similar compositions. The differences between the two dissolution curves are caused by the difference in their Fe concentrations. The somewhat higher Fe level in the ASCFS-2 alloy will increase the dispersion and thus accelerate the dissolution of the $CuAl_2$ particles under the same conditions of solution heat treatment. It is also interesting to note how the effects of Sr and Fe addition on the $CuAl_2$ phase counteract one another in comparing Figs 12, 13 and 14 for ASCF, ASCFS-1 and ASCFS-2 alloys, respectively.

The results obtained for the H4T1 alloy (industrial 319 alloy with Sr and P additions), Fig. 15, showed a different behavior, in that the dissolution of the $CuAl_2$ phase was found to be very sluggish in this alloy. After 8 hours of solution heat treatment, only 60% of the original amount of $CuAl_2$ phase observed in the structure was dissolved. Even after 100 hours, about 0.41% of the $CuAl_2$ phase remained undissolved. This observation is attributed to the presence of AlP particles that reinforce the segregation of $CuAl_2$ at the dendrite cell boundaries. The data for H20T1 alloy presented in Fig. 16 exhibits clearly that iron has the ability to neutralize this negative effect of phosphorus.

A summary of the above results is presented in Table VII, where the effects of the various element

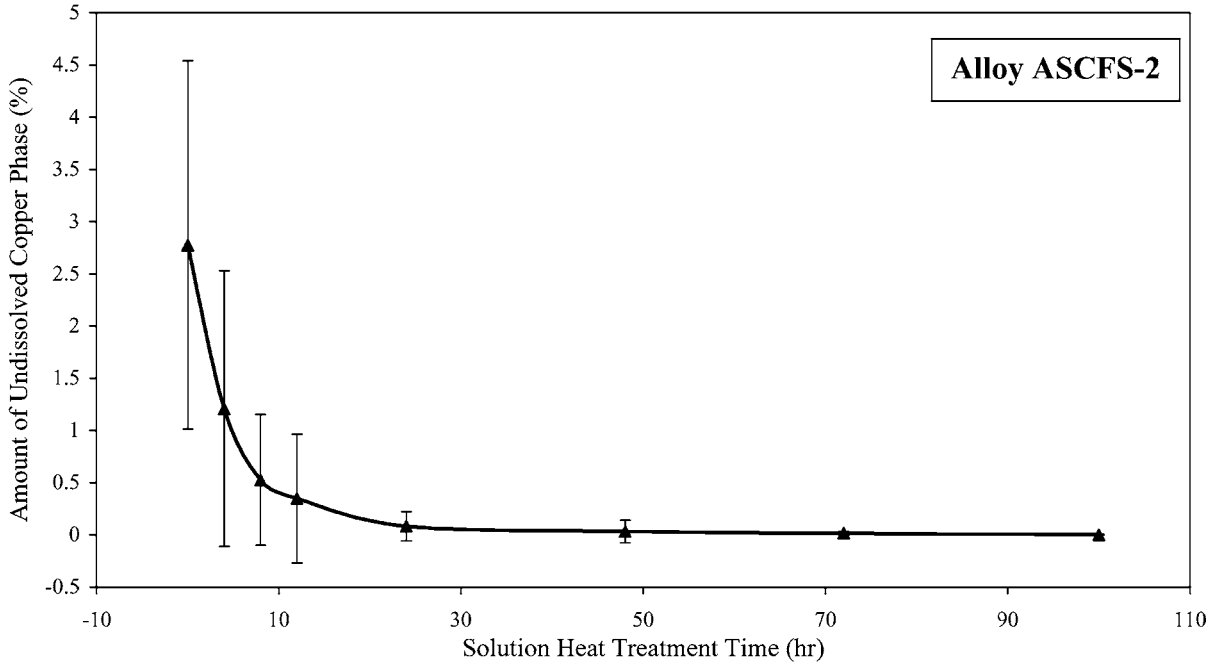

Figure 14 $CuAl_2$ phase dissolution in ASCFS-2 alloy during solution heat treatment at 505°C as a function of solution treatment time.

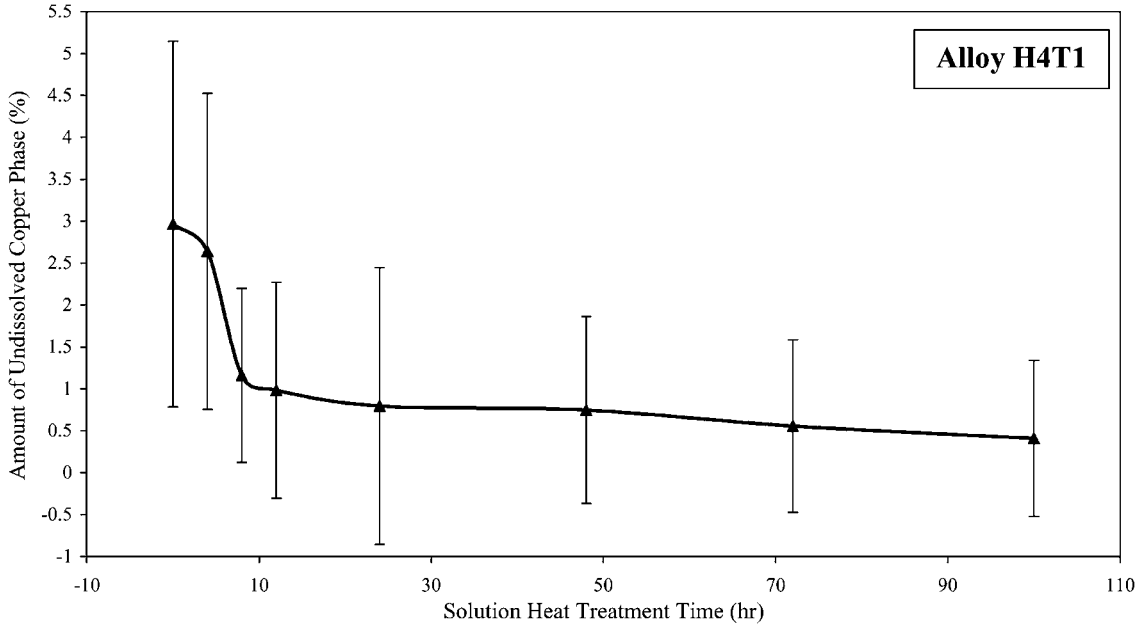

Figure 15 $CuAl_2$ phase dissolution in H4T1 alloy during solution heat treatment at 505°C as a function of solution treatment time.

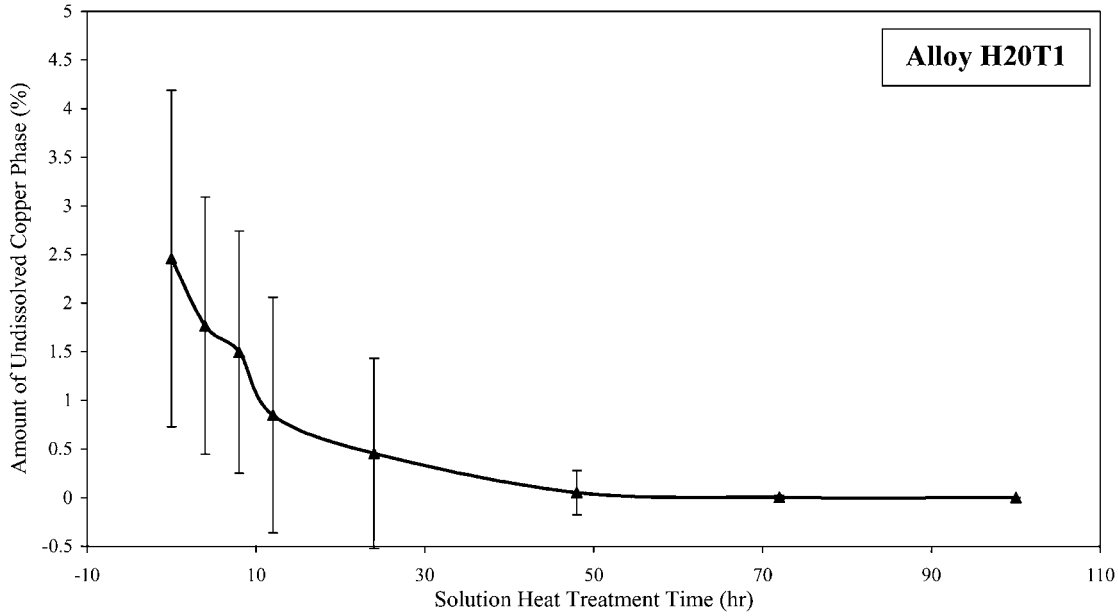

Figure 16 $CuAl_2$ phase dissolution in H20T1 alloy during solution heat treatment at 505°C as a function of solution treatment time.

additions on the dissolution of $CuAl_2$ as a function of solutionizing time are provided for the seven alloys studied, in terms of the amount of time required to reach 0.5% remaining $CuAl_2$ phase and complete dissolution. These results were obtained from the image analysis measurements; the Si particles were also observed to undergo morphological changes with the increasing solution heat treatment time. However, while the β-iron phase essentially retained its plate-like morphology, the dissolution of the platelets with increasing solution heat treatment time was also observed (as will be discussed at the end of the next section). These observations are in good agreement with the conclusions drawn by Crowell and Shivkumar [20].

TABLE VII Summary of dissolution of $CuAl_2$ phase at 505°C as a function of alloy composition and time

Alloy	Time to reach 0.5% of undissolved $CuAl_2$ phase (hr)	Time to reach approx. complete dissolution of $CuAl_2$ phase (hr)
ASC	8	48
ASCS	12	~100
ASCF	4–8	24
ASCFS-1	8–12	~72
ASCFS-2	8	~24
H4T1	>72	>100
H20T1	~20	~48

3.4. Electron probe microanalysis (EPMA)

Fig. 17 exhibits the two distinct forms of the copper phase: (a) the eutectic-like ($Al + CuAl_2$) phase, and (b) the blocky $CuAl_2$ phase that were observed in the present alloys. The EDX spectrum obtained from the $CuAl_2$ particles shown in (b) is given in Fig. 17c, in which strong reflections due to Al and Cu can be observed. The block-like morphology of the $CuAl_2$ phase

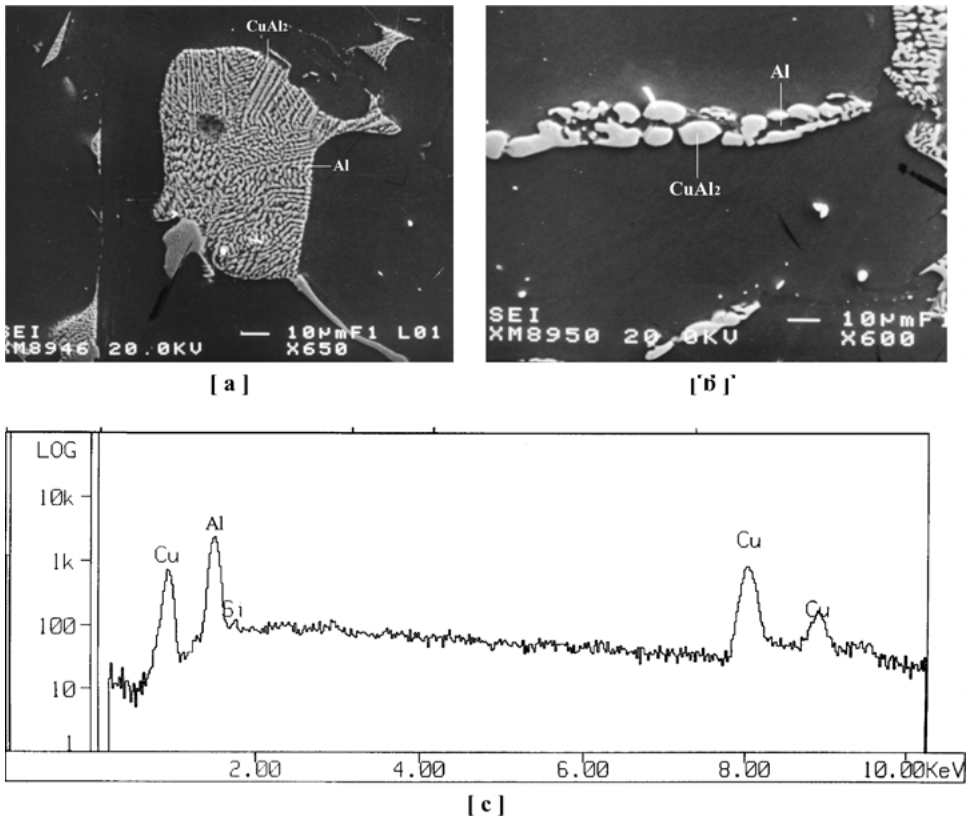

Figure 17 Backscattered images of (a) eutectic copper phase, (b) blocky copper phase, and (c) EDX spectrum obtained from $CuAl_2$ particles shown in (b), where strong reflections due to Al and Cu can be seen.

particles in Fig. 17b is clearly brought out when one compares it to the eutectic-like particles observed at the top right corner in the micrograph. The backscattered image of the as-cast microstructure of the Sr-modified H4T1 alloy in Fig. 18a clearly reveals the segregation of the copper phase particles in the interdendritic regions. The high magnification micrograph of Fig. 18b depicts details of the segregated region. It can be noted that due to the presence of Sr, the $CuAl_2$ phase particles precipitate mostly in the blocky form along the β-platelet sides. Fig. 18c shows the microstructure of H20T1 alloy (industrial 319 alloy containing Sr, Fe and 90 ppm P) after 8 hours solution heat treatment. As expected, some blocky $CuAl_2$ still exists in the microstructure, together with a scattering of fine $CuAl_2$ particles in the modified Si particle regions.

Fig. 19a shows the backscattered image of the H20T1 (33 ppm P) alloy sample, while Figs 19b and c depict the corresponding X-ray images of Al and P. The arrows in each case point to segregated block-like $CuAl_2$ particles. Figs 19d and e, taken at high magnification, show the X-ray images of Cu and P in the block-like $CuAl_2$ phase, respectively, where the diffusion of phosphorus inside these particles is clearly observed from the latter figure. The corresponding WDS analysis revealed that the maximum solubility of P in the copper phase did not exceed 0.1 at pct. As shown elsewhere [21], the block-like copper phase is believed to be nucleated by $(Al,P)O_2$ oxide particles.

The segregation of blocky $CuAl_2$ particles on the β-Al_5FeSi platelets in the as-cast ASCFS alloy is shown in Fig. 20. A high magnification backscattered image taken from ASCFS alloy (Fig. 21) illustrates the main process of fragmentation and dissolution of the $CuAl_2$ particles, which involves: (i) separation of the $CuAl_2$ particles from the β-phase after 8 hours solution heat treatment, followed by (ii) necking and spheroidization of the fragmented $CuAl_2$ particles, and (iii) radial diffusion of Cu atoms into the surrounding aluminum matrix.

The backscattered image taken from H4T1 alloy subjected to 8 hours solution heat treatment at 505°C reveals undissolved spheroidized $CuAl_2$ particles in a segregated region away from the Al-Si eutectic area (Fig. 22). It is interesting to note how the fine $CuAl_2$ particles scattered over the Si particles in Fig. 18c for the as-cast 319 alloy are almost absent after 8 h solution treatment.

Fig. 23 is a general view of the microstructure of H4T1 alloy after 100 h solution treatment at 505°C, revealing the almost complete dissolution of the $CuAl_2$ phase, although a few particles are still observed in the matrix. At the same time, it is also noticed that, during the process of dissolution, the Al and Cu concentrations in the $CuAl_2$ phase remain practically stable, as shown in Table VIII. Therefore, it may be suggested that the dissolution of the $CuAl_2$ phase occurs by diffusion of the Cu atoms in the outer layer of the $CuAl_2$ phase particles into the surrounding matrix, without changing the chemical composition of the remaining portions of the particles, even after 100 h at 505°C.

The line scans corresponding to ASCFS alloy following 8 h and 100 h solution heat treatment times are presented in Figs 24b and 25b, respectively, taken across

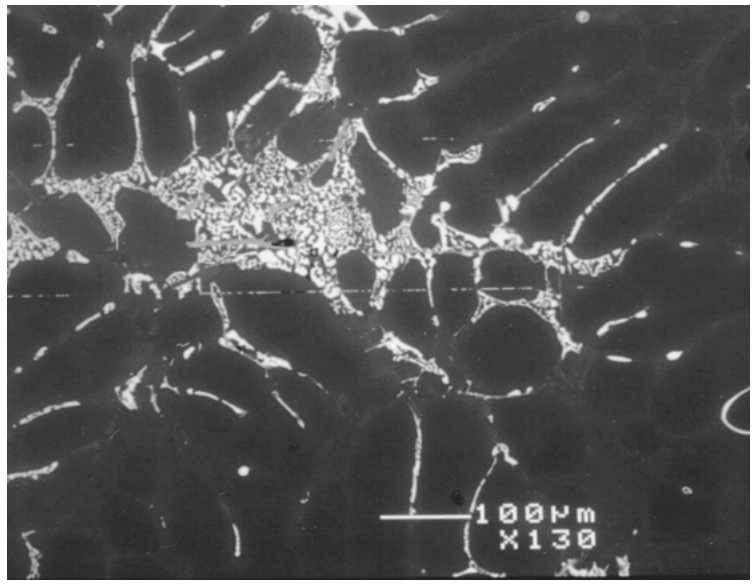

(a)

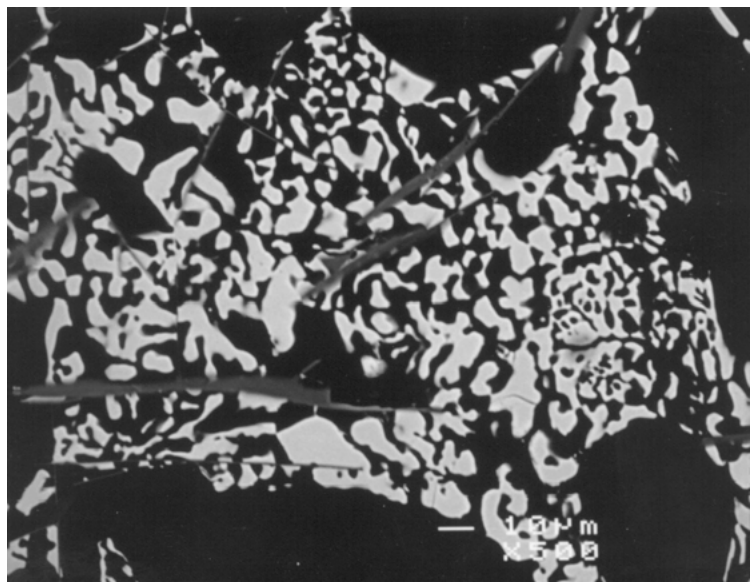

(b)

(c)

Figure 18 (a) Backscattered image of $CuAl_2$ phase distribution in as-cast H4T1 alloy, (b) high magnification micrograph of the Cu phase segregation area shown in (a), and (c) fine $CuAl_2$ particles scattering on the modified Si particles in as-cast H20T1 alloy.

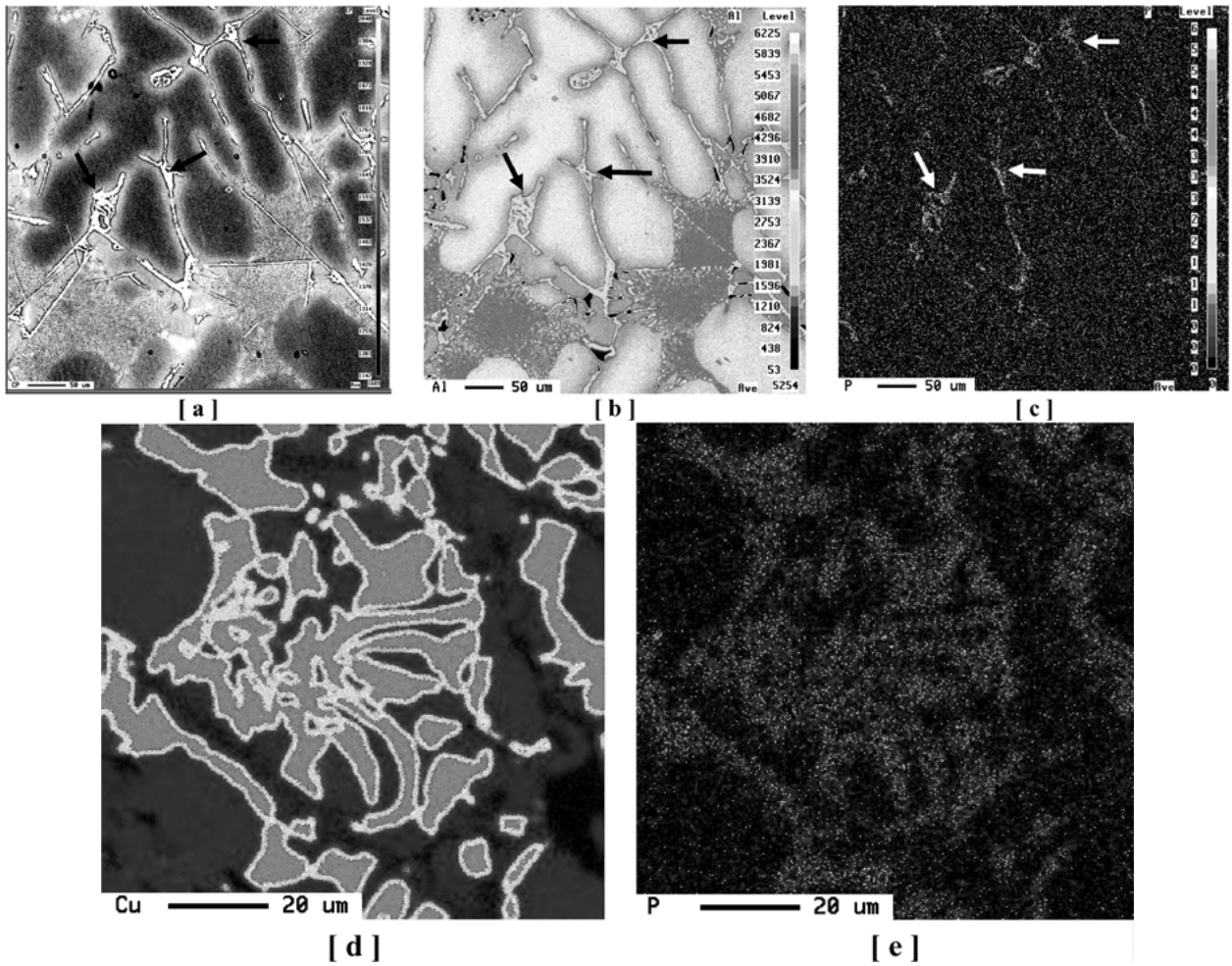

Figure 19 (a) Backscattered image, and X-ray images of (b) Al and (c) P underneath $CuAl_2$ particles observed in H20T1 alloy (ASC alloy containing Fe, P and Sr); high magnification X-ray images of (d) Cu and (e) P in the block-like $CuAl_2$ phase, taken from the same sample.

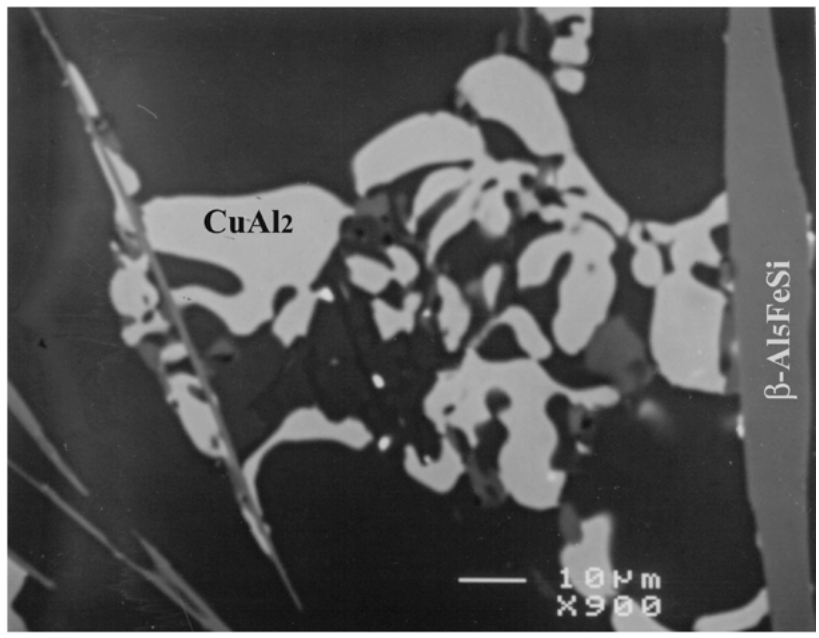

Figure 20 Microstructure of $CuAl_2$ particles precipitated on the β-plate in the as-cast ASCFS alloy.

the paths marked AB in the corresponding Figs 24a and 25a. These scans reveal the concentration gradients of Cu across the area containing the Cu-phase particles. The Cu concentration in the matrix around the $CuAl_2$ particles in Fig. 24b is ~4 wt% after 8 h solution treatment—much higher than the Cu concentration (~2 wt%) in the aluminum matrix after 100 h solution heat treatment, Fig. 25b. Thus, during the process of solution heat treatment, the Cu atoms diffuse in the matrix, far away from the remaining undissolved $CuAl_2$.

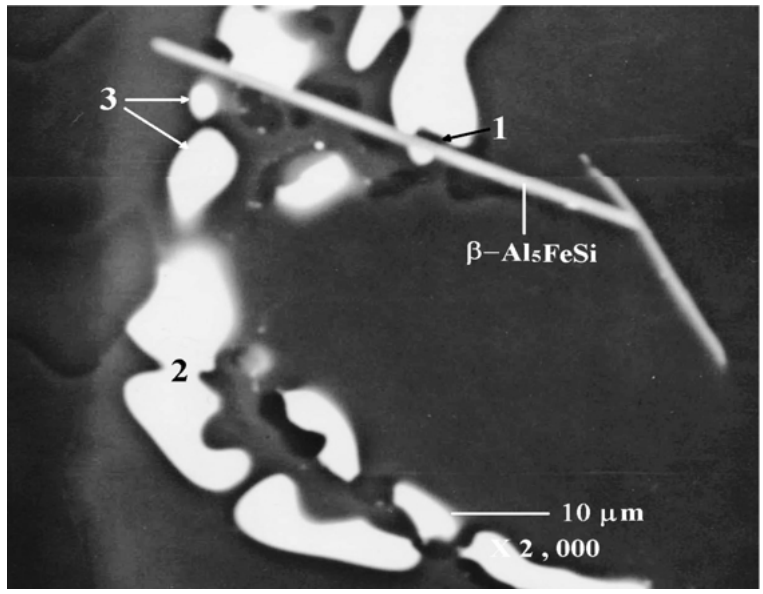

Figure 21 Backscattered image showing the dissolution process of $CuAl_2$ particles in ASCFS alloy after 8 h solution heat treatment at 505°C: (1) separation of $CuAl_2$ from β-plate, (2) necking of $CuAl_2$ cluster, (3) spheroidization of $CuAl_2$ and reduction in the size of $CuAl_2$ fragments.

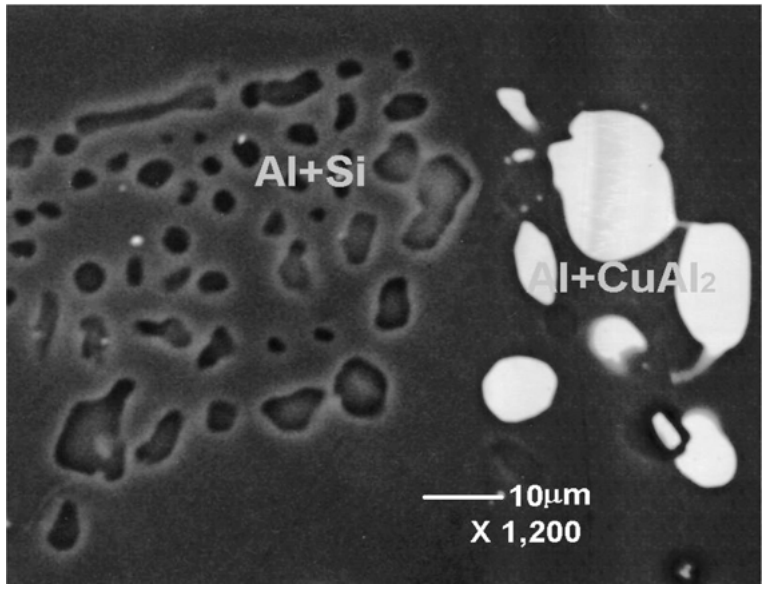

Figure 22 Backscattered image showing $CuAl_2$ dissolution in H4T1 alloy after 8 hours solution heat treatment at 505°C.

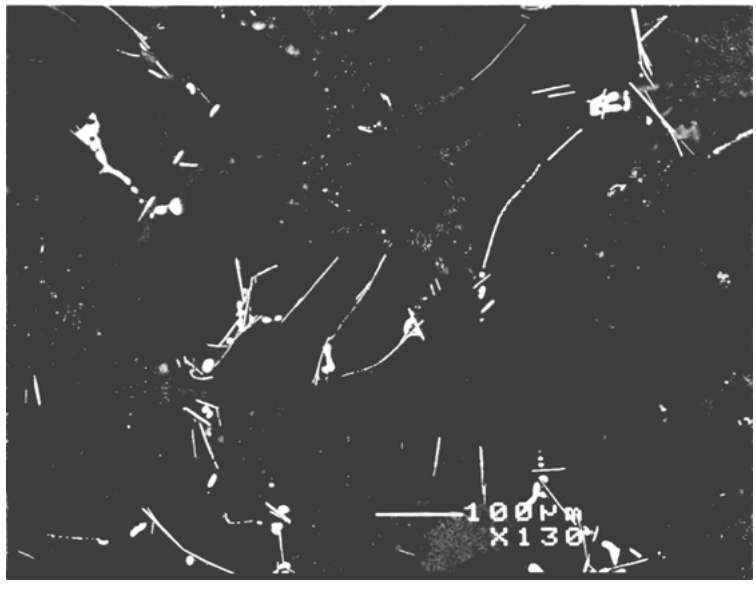

Figure 23 Backscattered image taken from H4T1 alloy after 100 hours solution heat treatment at 505°C.

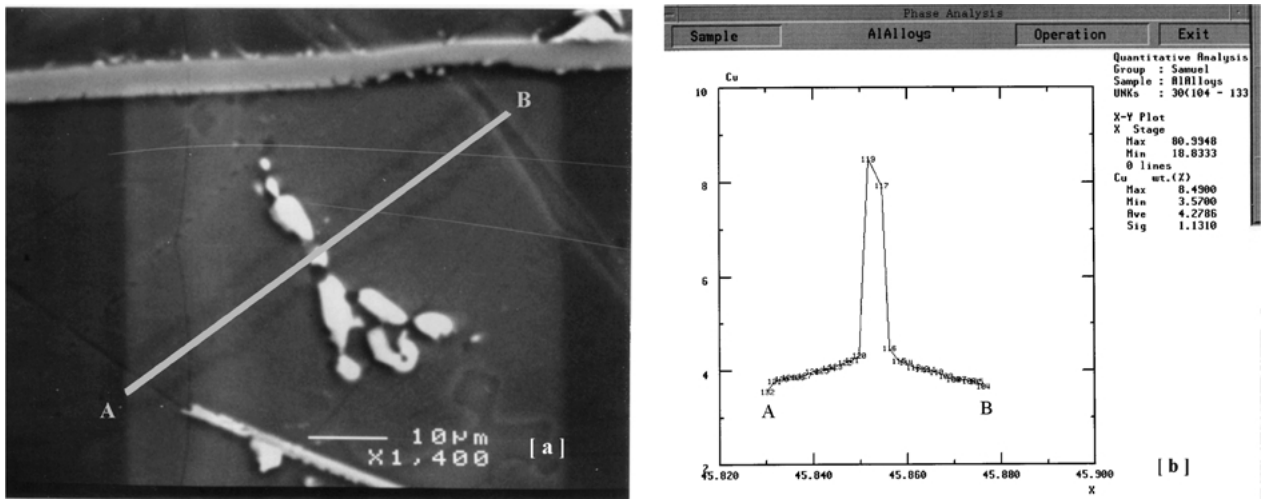

Figure 24 (a) Backscattered image of $CuAl_2$ particle in ASCFS alloy after 8 hours solution heat treatment; (b) the concentration profile of Cu along the path AB in (a).

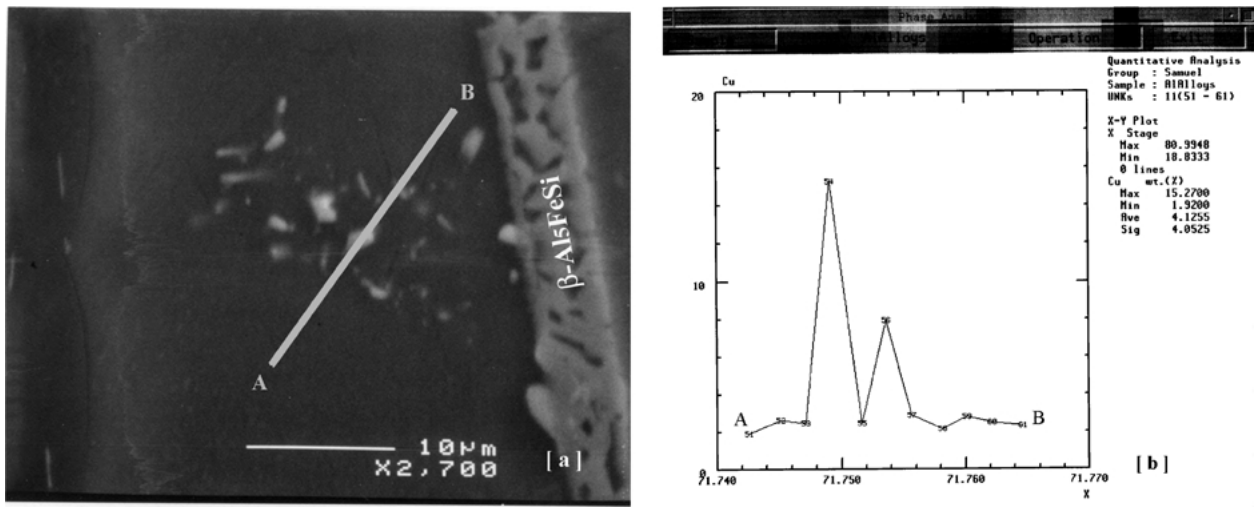

Figure 25 (a) Backscattered image of $CuAl_2$ particle in ASCFS alloy after 100 hours solution heat treatment; (b) the concentration profile of Cu along the path AB in (a).

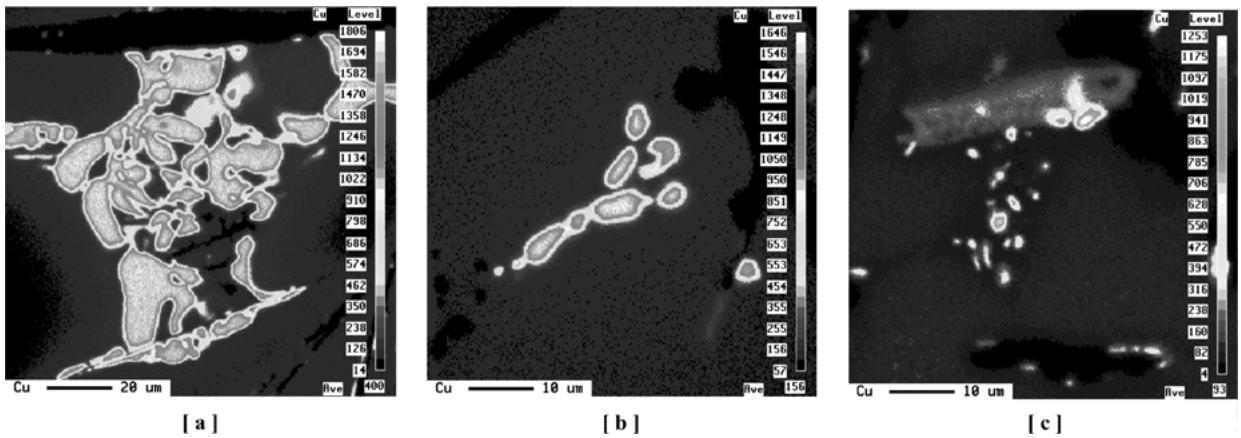

Figure 26 X-ray image of Cu in ASCFS alloy after: (a) 0 hr, (b) 8 hr and (c) 100 hr solution heat treatment at 505°C.

This is consistent with the X-ray image for Cu shown in Fig. 26, corresponding to the (a) as-cast, (b) 8 h solution-treated, and (c) 100 h solution-treated samples of ASCFS alloy. Table IX reveals the maximum Cu counts obtained from WDS analysis of ASCFS alloy shown in Fig. 26. Due to the diffusion of Cu during solution heat treatment, the maximum Cu concentration in the $CuAl_2$ particle shows a reasonable decrease. It is also interesting to note the sponge-like appearance of the β-phase shown in Fig. 25a, after 100 h solutionizing at 505°C, and compare it to the solid platelet seen in Fig. 20 for the as-cast condition.

TABLE VIII Al and Cu concentrations (at.%) in $CuAl_2$ phase particles during solution heat treatment at 505°C

Sr concentration (ppm)	Time of solution heat treatment (hr)	Al	Cu
0 (ASC)	0	68.647	29.285
	8	69.764	29.328
	100	69.287	28.267
200 (ASCS)	0	68.691	30.290
	8	68.941	30.118
	100	68.713	30.456

TABLE IX Maximum Cu counts obtained from WDS analysis for ASCFS alloy after different solution heat treatment times

Solution treatment time (hr)	Counts
0	1806
8	1646
100	1383

4. Conclusions

Based on our study of the effect of Sr, Fe and P element additions on the precipitation and dissolution of $CuAl_2$ phase in 319 type Al-Si-Cu alloys (following different solution heat treatment times at 505°C), the following conclusions can be made:

1. Addition of Sr leads to segregation of the copper phase in regions away from the Al-Si eutectic. This results in:
   i) an increase in the amount of blocky $CuAl_2$ in the as-cast alloy (~17.7%, cf. 2.60% in the unmodified alloy).
   ii) slowing down the rate of $CuAl_2$ dissolution on account of the $CuAl_2$ segregation during solidification.
2. Addition of Fe results in dispersion of the $CuAl_2$ phase and hence accelerates its dissolution during solution heat treatment. The precipitation of the β-Al_5FeSi phase provides nucleation sites for the precipitation of the copper phase, which, in turn, reduces the severity of $CuAl_2$ segregation. In this case, the blocky $CuAl_2$ form as small particles, which can be greatly beneficial in enhancing the $CuAl_2$ dissolution during solution heat treatment.
3. The $CuAl_2$ phase particles are more or less completely dissolved in the Al matrix after 100 hours solution heat treatment in all the alloys studied, except in the case of the 319 alloy containing both P and Sr, where the dissolution of the $CuAl_2$ particles is slowed down considerably during solution heat treatment. The presence of Sr leads to severe segregation of the $CuAl_2$ phase during solidification, whereas the negative effect of P is due to (a) its solubility in the $CuAl_2$ phase particles, and (b) the formation of $(Al,P)O_2$ oxide particles that act as nucleation sites for the precipitation of the block-like $CuAl_2$ phase. However, introduction of Fe to the alloy can assist in neutralizing this negative effect of phosphorus.
4. The mechanism for the dissolution of the $CuAl_2$ phase during solution heat treatment can be proposed as follows: (i) separation of the $CuAl_2$ phase particles from the β-Al_5FeSi platelets, (ii) necking of the $CuAl_2$ phase particles followed by spheroidization, (iii) dissolution of the spheroidized $CuAl_2$ particles by radial diffusion of Cu atoms into the surrounding aluminum matrix.

Acknowledgments

The authors would like to thank the Natural Sciences and Engineering Research Council of Canada (NSERC), the Fondation de l' Université du Québec à Chicoutimi (FUQAC), the Centre québecois de recherche et de développment de l'aluminium (CQRDA), General Motors Powertrain Group (U.S.A), and Corporativo Nemak (Mexico) for financial and in-kind support. Thanks are also due to MM. Glenn Poirier and S. Lang of the Microanalysis Laboratory, Earth and Planetary Science, McGill University for carrying out the EPMA analysis.

References

1. J. E. HATCH (ed.), "Aluminum: Properties and Physical Metallurgy," (American Society for Metals, Metals Park, OH, 1984) p. 143.
2. M. A. MOUSTAFA, F. H. SAMUEL, H. W. DOTY and S. VALTIERRA, *Int. J. Cast Metals Res.* **14** (2002) 235.
3. M. HANSEN, "Constitution of Binary Alloys," 2nd ed. (McGraw-Hill, New York, 1958) p. 84.
4. L. F. MONDOLFO, "Aluminum Alloys: Structure and Properties" (Butterworths, London, 1976).
5. A. COUTURE, *AFS Int. Cast Metals J.*, (1981) p. 9.
6. A. M. SAMUEL, A. PENNORS, C. VILLENEUVE, F. H. SAMUEL, H. W. DOTY and S. VALTIERRA, *Int. J. Cast Metals Res.* **13** (2000) 231.
7. P. N. CREPEAU, *AFS Trans.* **103** (1995) 361.
8. J. E. GRUZLESKI, F. PARAY, S. G. SHABESTARI and M. H. MULAZIMOGLU, *Al13: le Magazine de l'Aluminium* **2**(1) (1996) 23.
9. L. SHU-ZU and A. HELLAWELL, *Metall. Trans.* A **18A** (1987) 1721.
10. A. M. SAMUEL, P. OUELLET and F. H. SAMUEL, *AFS Trans.* **156** (1997) 951.
11. D. ARGO and J. E. GRUZLESKI, *ibid.* **96** (1988) 65.
12. G. K. SIGWORTH, S. SHIVKUMAR and D. APELIAN, *ibid.* **97** (1989) 811.
13. M. DJURDJEVIC, T. STOCKWELL and J. SOKOLOWSKI, *Int. J. Cast Metals Res.* **12** (1999) 69.
14. F. H. SAMUEL, A. M. SAMUEL and H. W. DOTY, *AFS Trans.* **104** (1996) 893.
15. J. GAUTHIER, P. R. LOUCHEZ and F. H. SAMUEL, *Cast Met.* **8**(1, p. 1) (1995) 91.
16. *Idem.*, *ibid.* **8**(1, p. 2) (1995) 107.
17. J. H. SOKOLOWSKI, X.-C. SUN, G. BYCZYNSKI, D. O. NORTHWOOD, D. E. PENROD, R. THOMAS and A. ESSELTINE, *Journal of Materials Processing Technology* **53**(1-2) (1995) 385.
18. A. M. SAMUEL, J. GAUTHIER and F. H. SAMUEL, *Metall. Mater. Trans. A* **27A** (1996) 1785.
19. S. SHIVKUMAR, S. RICCI, JR. and D. APELIAN, in "Production and Electrolysis of Light Metals," edited by B. Closset, (Pergamon Press, New York, 1989) 173.
20. N. CROWELL and S. SHIVKUMAR, *AFS Trans.* **103** (1995) 721.
21. Z. LI, A. M. SAMUEL and F. H. SAMUEL, *J. Mater. Sci. Letters* (2002) in press.

Received 9 April
and accepted 30 October 2002